Research Article

Experimental Investigation of Impact Localization in Composite Plate using newly Developed Imaging Method

Mohammad Faisal Haider [1, *], **Asaad Migot** [1], **Md Yeasin Bhuiyan** [1] and **Victor Giurgiutiu** [1]

[1] Department of Mechanical Engineering, University of South Carolina, 300 Main Street, Columbia, SC 29208

* Correspondence: haiderm@e-mail.sc.edu; Tel.: +1-803-777-0619

Abstract: This paper focused on impact localization of composite structures, which possess more complexity in the guided wave propagation because of the anisotropic behavior of composite materials. In this work, a composite plate was manufactured by using a compression molding process with proper pressure and temperature cycle. Eight layers of woven composite prepreg were used to manufacture the composite plate. A structural health monitoring (SHM) technique is implemented with piezoelectric wafer active sensors (PWAS) to detect and localize the impact on the plate. There are two types of impact event are considered in this paper (a) low energy impact event (b) high energy impact event. Two clusters of sensors recorded the guided acoustic waves generated from the impact. The acoustic signals are then analyzed using a wavelet transform based time-frequency analysis. The proposed SHM technique successfully detect and localize the impact event on the plate. The experimentally measured impact locations are compared with the actual impact locations. An immersion ultrasonic scanning method was used to visualize the composite plate before and after the impact event. A high frequency 10 MHz 1-inch focused transducer was used to scan the plate in the immersion tank. Scanning results show that there is no visible manufacturing damage in the composite plate. However, clear impact damage was observed after the high-energy impact event.

Keywords: impact localization, composite materials, PPS, imaging method, immersion ultrasonic scanning

1. Introduction

Advanced composites are increasingly being used in many applications [1–4]. However, the prognosis of their long-term behavior is still an active area of research. The ability to predict functional life depends upon characterizing and predicting the evolution of the material state of the structure (e.g., distributed damage development, accumulation, and interaction) which affect global property (strength and stiffness) degradation and eventual failure. The lack of monitoring of that local damage often results in empiricism, limiting innovation in the use of composite materials. Therefore, appropriate nondestructive inspection (NDI) and structural health monitoring (SHM) technique are in urgent need for composites structure [5–7]. The maintenance costs associated with the aging infrastructure becoming an ongoing concern. In addition to maintenance cost, downtime of those structures makes the economy more inviable. SHM may alleviate this economy barrier by (a) assessing the state of the structure beforehand and do the on-site maintenance with minimum downtime and (b) ensuring increased safety and reliability while reducing maintenance costs. For new structures, the embedded sensors and sensing systems from the design stage are likely to reduce the overall life-cycle cost. [8]. SHM has been implemented for composites using a built-in sensor network [8,9] and real-time pipeline integrity monitoring [11].

The acoustic events can be from many different sources such as (a) impact of a foreign object (bird strike, debris hit) [12] (b) fatigue crack generation in the structures [13], (c) matrix cracking, fiber

breakage and/or delamination of the composites. The detection, localization, and sizing of the damage from all these events is an essential area of SHM [14–16]. These acoustic events mostly generate the waves in an ultrasonic regime [17]. These waves propagate in the structures and carry the information of the acoustic events. Now the research question is: how can one capture these waves and extract damage-related information?

Undetected impact damage has a long track record of causing severe failure to composite structures. The impact damage from airport debris caused Concord to fly miserably and led to disaster. Hitting by debris or any foreign object is very common for moving structures, and after any such hit, the structure should be adequately inspected especially near the impact location. Therefore, this impact location must be identified by an appropriate acoustic source localization method. After identifying the impact region, a more careful active SHM can be performed to conclude the severity of the damage caused by such impact [18,19]. Active SHM has been implemented to quantify the damage [20], and a non-contact approach has been implemented in pipeline defects [21]. However, these research mainly focused on aluminum alloys.

In this research, a comprehensive study has been carried out starting from the manufacturing the composite plate to final impact detection and localization using SHM approach. A composite plate was manufactured from woven carbon fabric prepreg by using a compression molding process. An SHM technique has been implemented to detect and localize the impact event by using permanently bonded piezoelectric wafer active sensors in the manufactured composite plate. We found that the experimental measurements are in good agreement with actual impact localization. The manufactured composite plate was tested nondestructively using immersion ultrasonic scanning. The scanning results showed that the plate had a minimal to no manufacturing defect that can affect the impact detection and localization.

2. Composite plate manufacturing using compression molding process

Polyphenylene Sulfide (PPS) fabric prepreg (TC1100) from TenCate Cetex was used to manufacture the thermoplastic composite (TPC) plate. The PPS prepreg was a pre-consolidated reinforced laminate with continuous woven carbon fibers. TC1100 is pre-consolidated reinforced laminate (RTL) utilizing continuous woven carbon fibers (Carbon T300 3K).

(a)   (b)
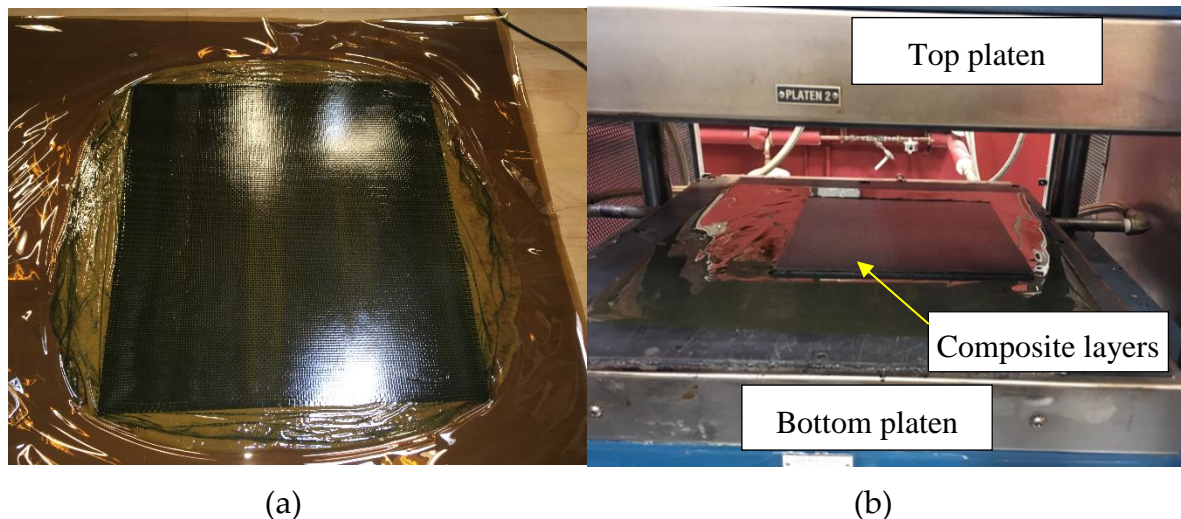
Figure 1. Composite layers (a) with thin protective films (b) in the compression-molding machine

The prepreg was cut to the desired shape (square in this case) with a dimension of 305 mm by 305 mm (12 inches by 12 inches). Each cutting section served as a layer. Eight layers of woven fabric then stacked upon each other to form a laminate. Two thin protective films of plastics with a very high melting point were used on top and bottom of the stack up (**Figure 1** a)). The laminate of eight layers was then placed between two flat platens of the compression-molding machine as shown in

80 **Figure 1**(b). The melting temperature of the PPS fabric is 536^{0}F. Hence, a cure cycle must contain a
81 temperature higher than the melting point for proper melting and flow of the resin. **Figure 2** (a) shows
82 a standard cure cycle used for this laminate. A constant pressure of 150 psi was applied during the
83 cure cycle. Heating was adjusted in the compression-molding chamber for raising the laminate
84 temperature to 610^{0}F within 45 minutes. Then the temperature of the laminate dwelled at 610^{0}F for
85 30 minutes. At the end of dwell time, the laminate was air cooled from 610^{0}F to room temperature in
86 30 minutes. After the cure cycle completed in about 2 hours, the laminate was taken out from the
87 platen. The extra resin flow at the edges of the laminate was trimmed. **Figure 2** (b) shows the final
88 composite laminate after the trimming process. The resulting plate had a thickness of 1.6-mm. The
89 dimension of the final composite plate was 387 mm by 276 mm (11.3 inches by 10.9 inches).

(a)   (b)
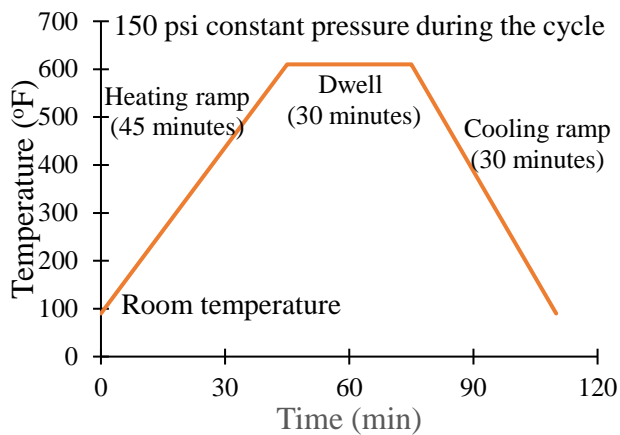
90 **Figure 2.**   (a) Cure cycle for the PPS prepreg (b) Final composite plate

91 **3. Impact detection and localization using SHM technique**

92 The impact is a common damage situation that can occur in real-life structures. In this
93 experiment, a structural health monitoring (SHM) technique is implemented to detect and localize
94 the impact. Six lead zirconate titanate (PZT) piezoelectric wafer active sensors (PWAS) are
95 permanently bonded to the composite plate. Each PWAS transducer is 7-mm in diameter and 0.5-mm
96 in thickness [22].

97 *3.1. Developing Imaging method*

98 We developed a new imaging method of acoustic source localization in anisotropic plates due
99 to impact event. In this method, the two clusters of sensors (every cluster has three sensors) were
100 used to localize the impact points as shown in the **Figure 3**. To localize the impact point using imaging
101 methods, we divided the region of interest into small pixels. The first step of this imaging approach
102 is to determine the slope values for every cluster based on the time of flight of impact signals received
103 by the clusters sensors [23, 24]

$$\mathrm{Slope}^1 = \frac{\Delta t_{23}}{\Delta t_{21}}$$

$$\mathrm{Slope}^2 = \frac{\Delta t_{56}}{\Delta t_{54}}$$

104   (1)

105 Where Slope^1 and Slope^2 are slope values of Cluster1 and Cluster2. Δt_{23} is the difference in time
106 of flight between sensors S_2 and S_3.

107

108
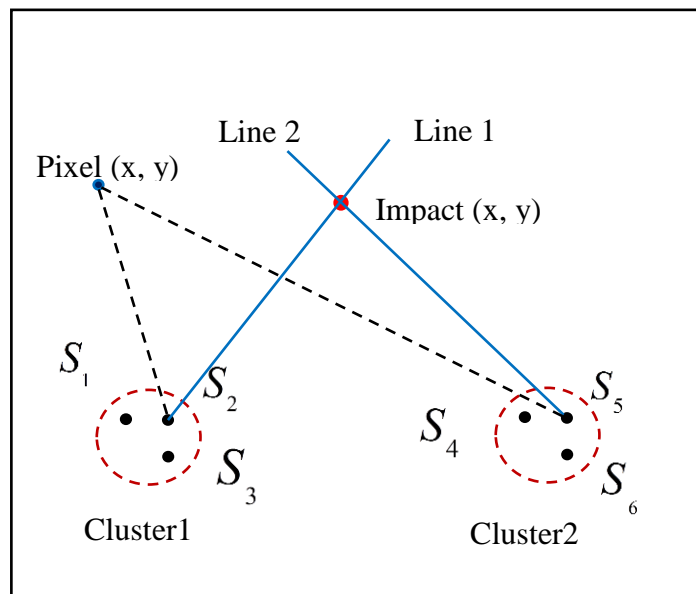
Figure 3.   Mapping of two lines from each cluster to show the intersection at the impact
location

109
110

111   The second step is to determine the slope values for every pixel of the interested area for a particular
112   sensing path line of a particular cluster as follow

$$\text{Slope}_{ij}{}^1 = \frac{y_2 - y_i}{x_2 - x_j}$$

$$\text{Slope}_{ij}{}^2 = \frac{y_5 - y_i}{x_5 - x_j}$$

113   (2)

114   where $(x_2, y_2), (x_5, y_5)$ are the coordinates of sensors S_2 (in Cluster1) and S_5 (in Cluster2)
115   respectively. To determine the pixels field values for every individual path, we use Gaussian
116   distribution equation

$$f_{ij}^k(x, y) = \frac{1}{\sigma\sqrt{2\pi}} e^{-\frac{(x-\mu)^2}{2\sigma^2}}$$

117
118   (1)

119   where $f_{ij}^k(x, y)$ is the field value of every pixels $P(x, y)$ of the image for a particular sensing path
120   line (for a particular cluster), x represents the slope value at each pixels $Slope_{ij}^k$ for the sensing
121   path line of $Cluster\,k$, μ represents the slope value for the sensing path line of $Cluster\,k$ which
122   can be determined experimentally based on the time of flight values of cluster sensors. The standard
123   deviation, σ which describes the variability or dispersion of a data set, which was taken as a
124   function of slope value. In this work, the σ values were taken between 0.02-1 (the σ value needs to
125   be increased with increasing the slope value and vice versa). The k represents the order of used
126   cluster. To fuse all the images from different sensing paths, summation and/or multiplication
127   algorithm were used [10, 25] following the equations below:

$$P_{sum}(x, y) = \sum_{k=1}^{N} f_{ij}^{k}(x, y)$$

128

(2)

$$P_{mult}(x, y) = \prod_{k=1}^{N} f_{ij}^{k}(x, y)$$

129
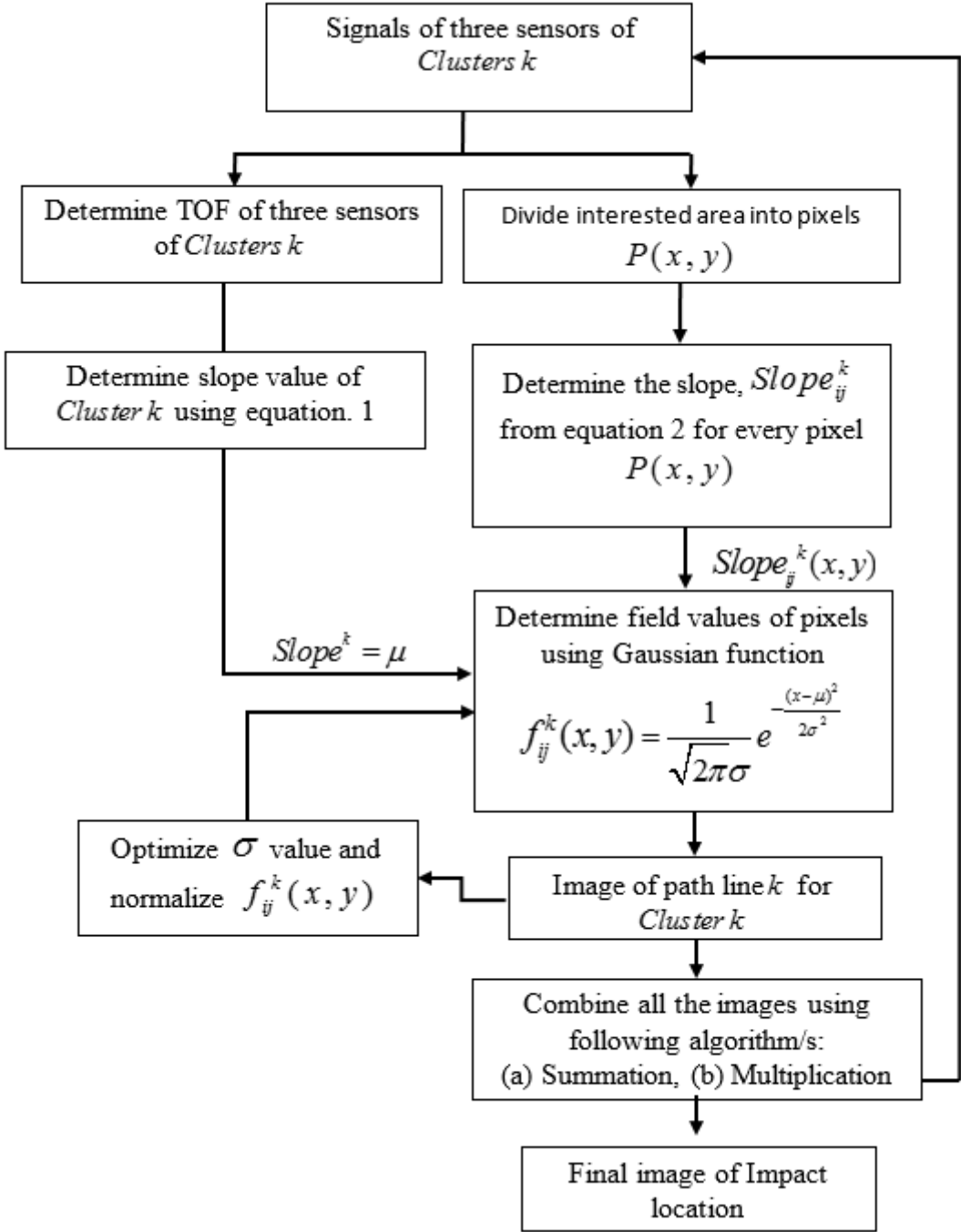
130

131   **Figure 4.** Flowchart of the developed imaging method

132   where $P_{sum}(x, y), P_{mult}(x, y)$ are   the   total   field   values   of   each   pixels   using   a   summation   or
133   multiplication algorithm. N represents the total number of sensing paths lines which equal to the
134   total number of clusters. In this work, we have used two clusters. Two-lines paths from each cluster

135 are mapped over the pixels and intersected at the impact point as shown the **Figure 3**. **Figure 4** shows
136 the details procedure of imaging method.

3.1 *SHM experimental setup for impact detection and localization*

138   The experimental setup is shown in **Figure 5**. Two clusters of PWAS sensors were used as named
139 Cluster1 (at coordinate location (60, 53)) and Cluster2 (at coordinate location (197, 53)). In each cluster,
140 there were three PWAS transducers placed at 90 deg. Orientation. These configuration of sensors are
141 especially useful when one does not know the exact material properties of the plate. This method can
142 accurately predict the location of the impact by analyzing the received signals by the sensors without
143 knowing the material properties. Signals from an impact location were received through six sensors
144 using two oscilloscopes (**Figure 5**).

Zoom in view of the plate
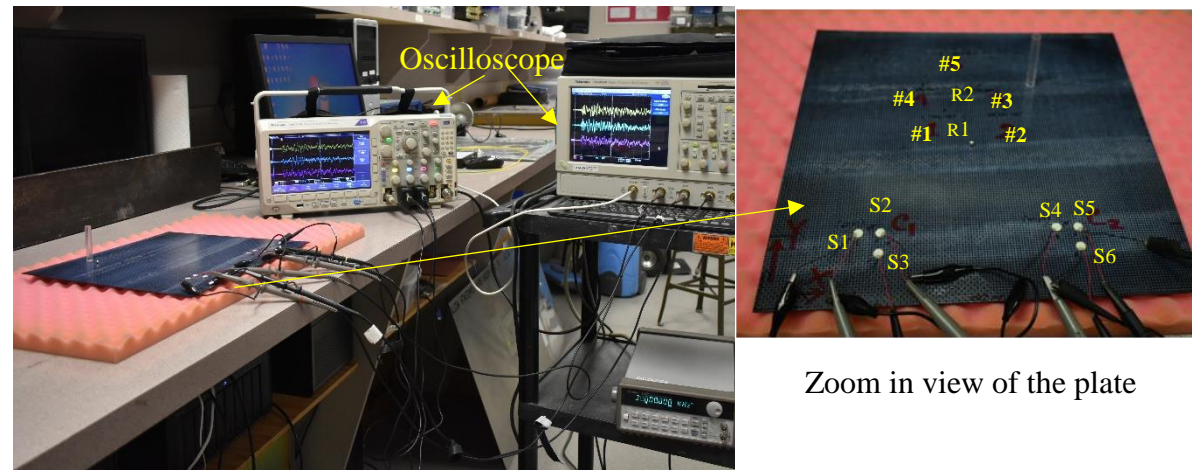
145   **Figure 5.** Experimental setup for impact detection and localization on the composite plate

3.2 *Low-energy impact method*

147   The plate was subjected to impact by a steel ball at five different locations. The diameter of the
148 steel ball is 4.5 mm. The weight of the steel ball is 0.33 kg. The steel ball was freely impacted from
149 0.05 m height following a special guide fixture to create 0.16 J impact energy. The five impact locations
150 are marked by #1, #2, #3, #4, and #5 in **Figure 5**. At each location, three impact events were created to
151 check the repeatability of the test. When the steel ball hit the plate, it generates acoustic emissions.
152 The energy of acoustic emission (AE) propagates as guided waves in the plate. The guided waves
153 produce stress and strain waves in a plate. The permanently bonded PWAS transducers captured the
154 strain waves. Since the six PWAS transducers were located at different distances, the time of flights
155 (TOF) of the received signals was different.

3.2.1. Experimental Signal Analysis and Impact Detection

157   The six signals from the six sensors are illustrated in **Figure 6**. **Figure 6** corresponds to the signals
158 received from impact location#3. Only the low-energy impact at location #3 is presented here as a
159 representative result. These signals received by the sensors indicate that there was an impact event.
160 In this experiment, low energy impact (height was intentionally kept low) was used to show how
161 sensitive the proposed SHM system is. In case of high energy impact, it would be much easier to
162 detect the impact event since it would produce higher amplitude AE signals.

163
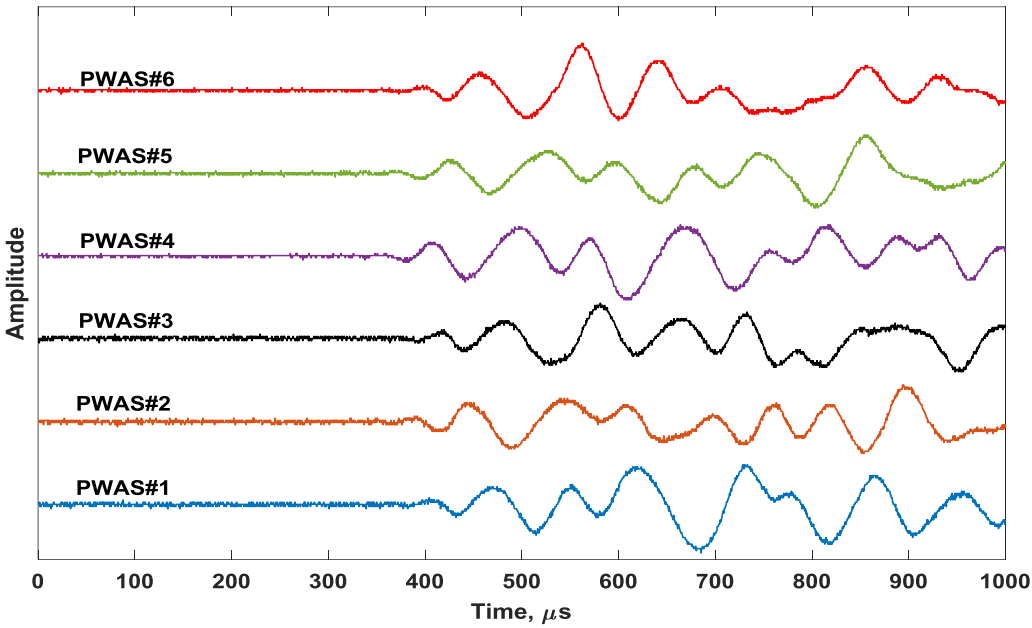
164   **Figure 6.** PWAS recorded acoustic signals due to low-energy impact at location #3 (150, 200) mm

165   3.2.2. Low-energy impact Localization

166   To localize the impact event in the plate, it is essential to determine the time-of-flight correctly.
167   Just by looking at the time-domain signals, often it is hard to determine the time of flight. The accurate
168   way is to use a signal processing method to determine TOF. A wavelet transform based method was
169   used in this paper to determine the TOF. The wavelet transform based method is demonstrated in
170   **Figure 7**. As an example, two PWAS signals received from impact event # 3 are considered.
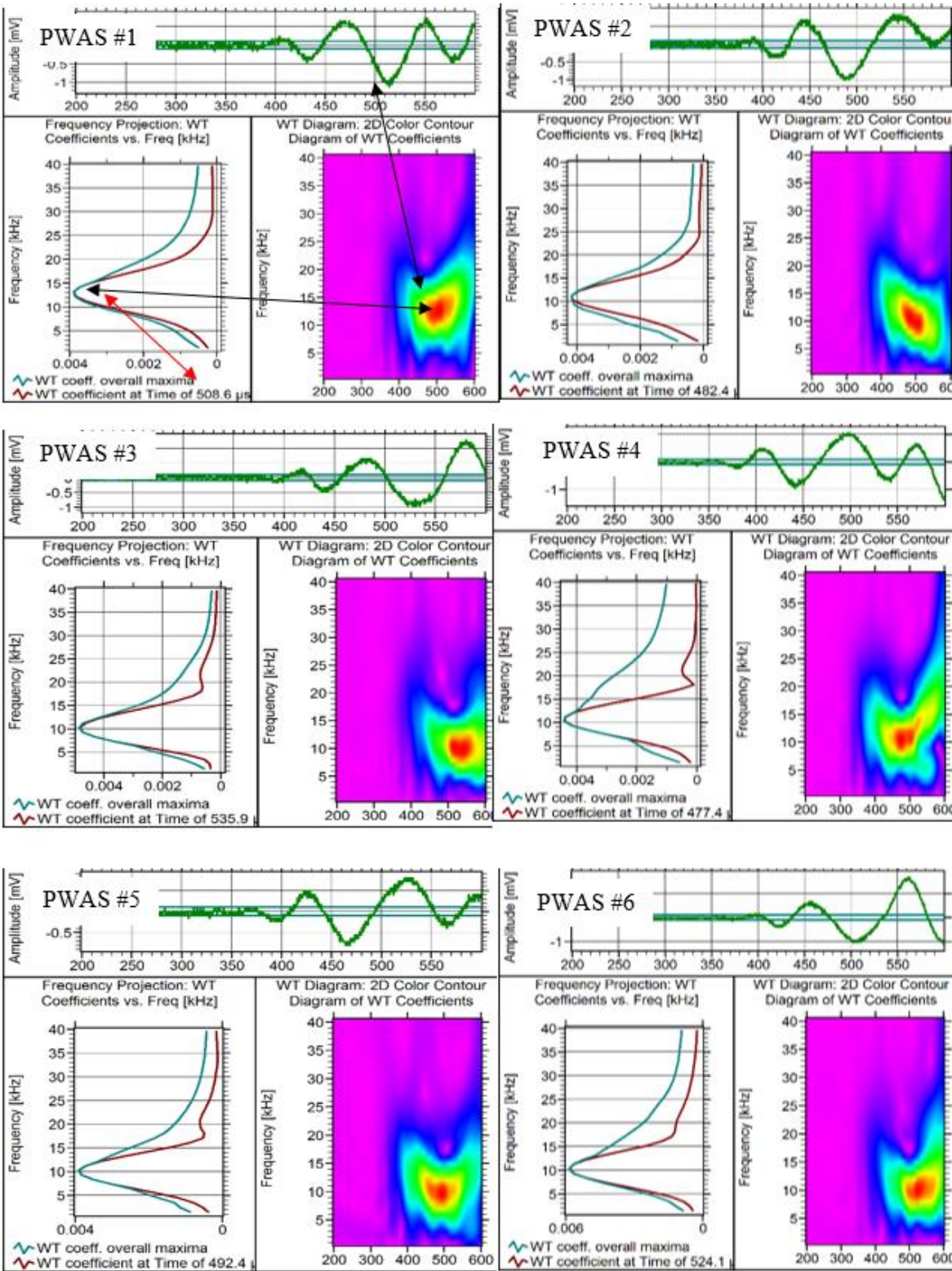
Figure 7. Wavelet transform of the PWAS recorded signals to determine the time of flight (TOF)
(for low-energy impact location #3)

In wavelet transform (WT), adjustable windows can better keep track of time and frequency
information as compared to short-time Fourier transform (STFT), another popular method. WT can
zoom in on short bursts and zoom out to detect long, slow oscillations by auto adjustment of the
windows. Since the nature of the signal is unknown during an impact, WT provides more accurate
information from the time-frequency analysis. A freeware Vallen software [26] was used to perform
WT on the signals. This program has a Gabor function as the "mother" wavelet.
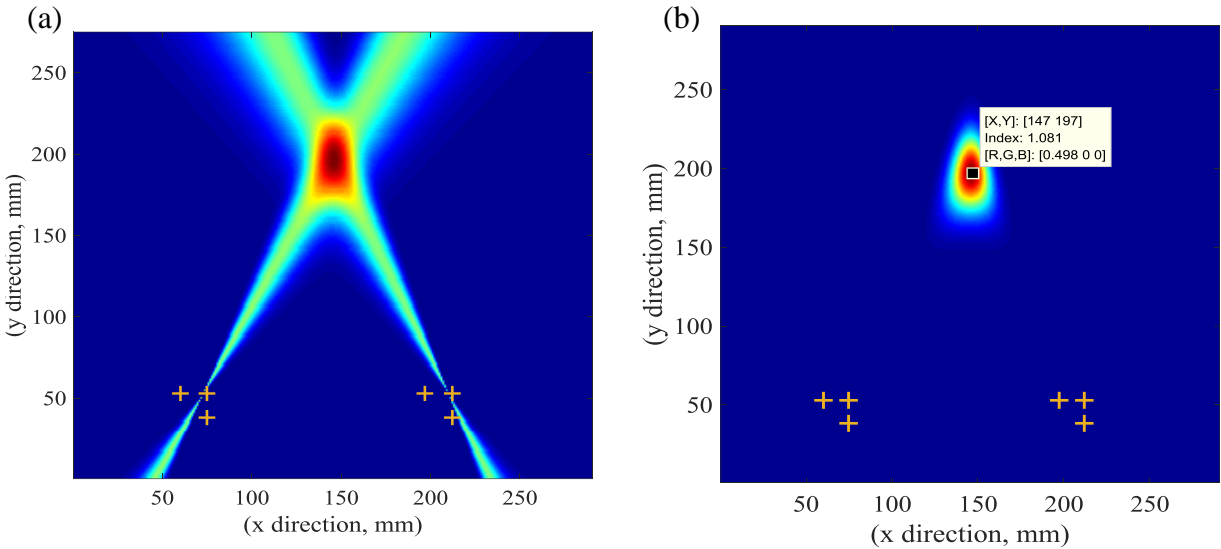
Figure 8. Imaging results of localization low-energy impact at point #3 (150, 200) mm using imaging methods; (a) summation method; (b) multiplication method

Table 1 Experimental measurement vs. actual location of the low-energy impact

Impact event	Actual location (x, y) mm	Measured location (x, y) mm	% of error (Based on sensor cluster 1)
#1	(120, 170)	(117.7, 161.9)	6.7%
#2	(170, 170)	(166, 163.8)	4.8%
#3	(150, 200)	(147.4, 197.8)	1.9%
#4	(100, 200)	(101.8, 195.5)	2.7%
#5	(130, 250)	(131.7, 251.6)	0.9%

The WT diagrams in **Figure 7** show the frequency-time plot using the WT. It shows the amplitude mapping over various frequencies and time. At each time and frequency, a WT coefficient variation can be plotted as shown on the bottom-left of each box. An overall maximum of the WT coefficient has been plotted. The time at which the WT profile matches the overall WT maxima provide the TOF. This process has been repeated for all PWAS signals to determine the TOFs.
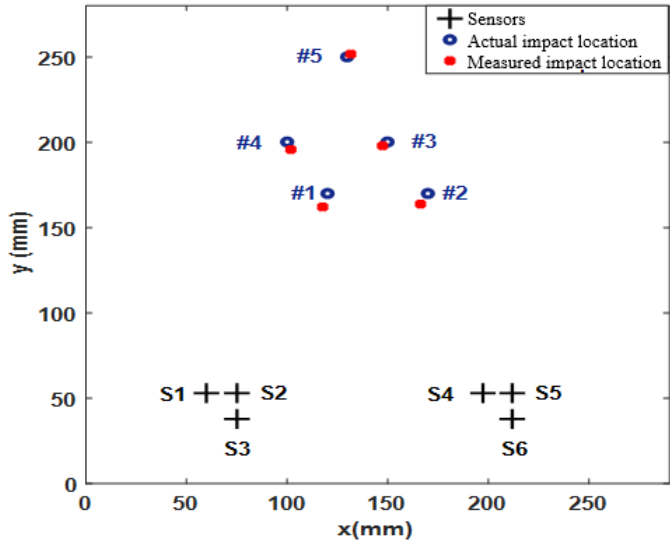
Figure 9. Experimentally measured low-energy impact location and actual impact location on the manufactured composite plate

191 Once the TOFs for all the AE signals were known, a localization algorithm was used to determine the
192 impact location. The imaging method is described in the earlier section (Section 3.1). The results from
193 the imaging method are illustrated in **Figure 8**. The experimental measurement and the actual impact
194 location is summarized in **Table 1**. The visual representation of the actual impact location and
195 measured impact location is shown in **Figure 9**. It shows that the experimentally measured impact
196 locations are in good agreement with the actual impact location.

197 *3.3 High-energy impact method*

198 In this section, impact localization was done due to high energy impact. The plate was subjected
199 to impact by a sharp point cylinder at two different locations. These locations are marked by R1 and
200 R2. The projectile diameter of the sharp point cylinder is 4.5 mm. The weight of the cylinder is 0.920
201 kg. The sharp point cylinder was freely impacted from 1m height following a special guide fixture to
202 create 9 J impact energy. The six signals from the six sensors are illustrated in **Figure 10**. **Figure 10**
203 corresponds to the signals received from impact location R1.
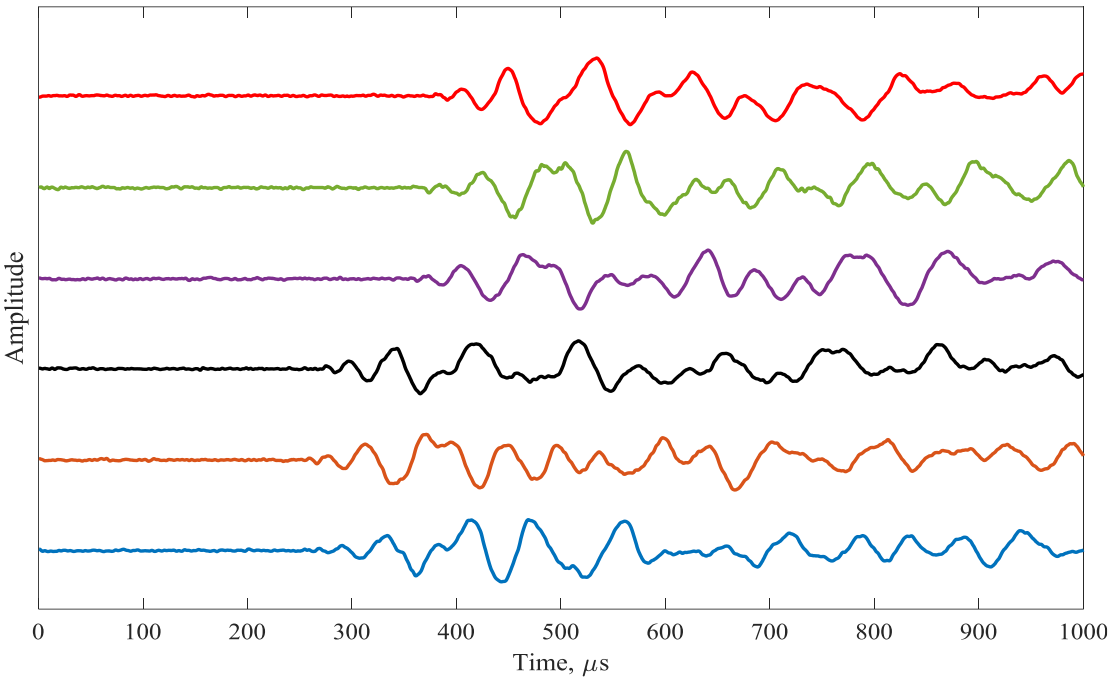
204
205 **Figure 10.** PWAS recorded acoustic signals due to the high-energy impact at location #R1 (128, 167
206 mm)

207 A wavelet transform based method was used to determine the TOF as described in the previous
208 section (section 3.2.2). **Figure 11** illustrates the impact location of high-energy impact using the
209 developed imaging method. The experimental measurement and the actual impact location is
210 summarized in Table 2. It can be observed from Table 2 that the impact location determined by the
211 current approach is very accurate compared to the actual impact location.

(a)   (b)
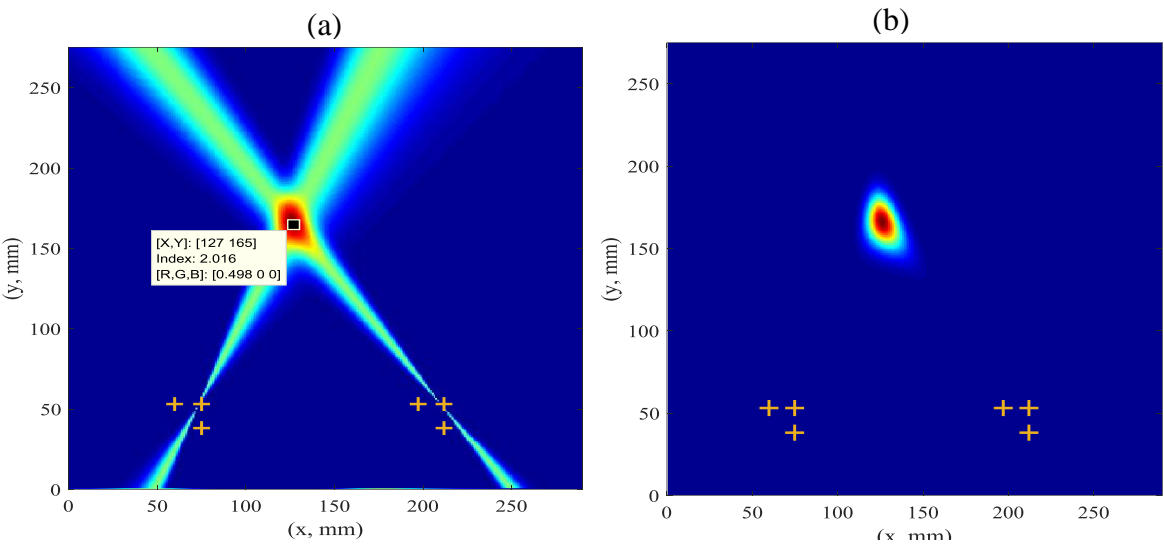
Figure 11. Imaging results of localization high-energy impact at point #R1 (128, 167) mm using imaging methods; (a) summation method; (b) multiplication method

Table 2   Experimental measurement vs. actual location of the high-energy impact

Impact event	Actual location (x, y) mm	Measured location (x, y) mm	% of error (Based on sensor cluster 1)
#1	(128, 167)	(127, 165)	2.4%
#2	(147, 207)	(146, 204)	2.8%

4. Nondestructive inspection (NDI) of the composite plate using immersion ultrasonic testing

An ultrasonic nondestructive inspection (NDI) was performed on the manufactured composite plate before and after the impact event. The purpose of this NDI was to verify if there is any major flaws, delamination or defects during the manufacturing process and to visualize the damage after the impact. An immersion ultrasonic scanning was performed on the plate, which can detect defects or delamination across its thickness. The ultrasonic immersion tank is used to inspect the composite specimen. This device can be used to identify the internal porosity, detect and size of delamination and other types of defects.
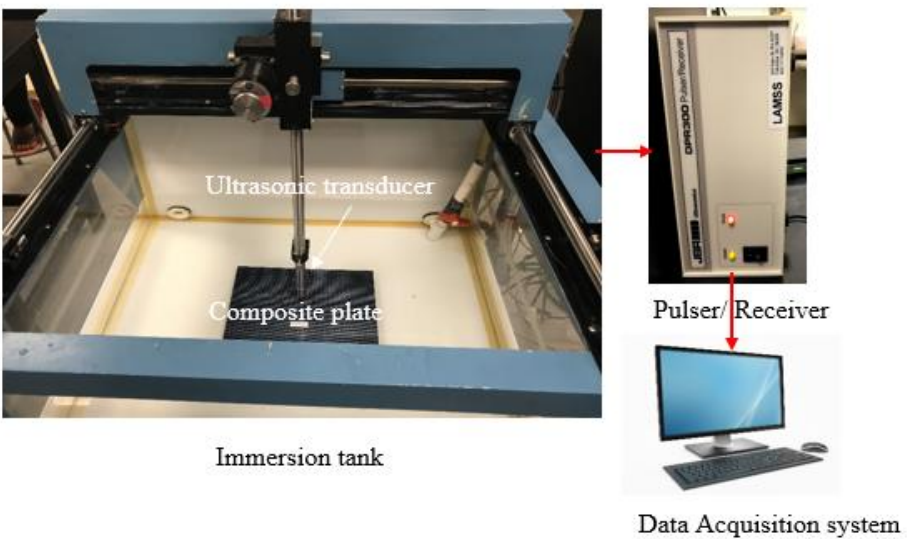
Figure 12. Experimental setup for the ultrasonic inspection of composite plate under water

225   In immersion testing, the transducer is placed in the water, above the test object, and a beam of sound
226   is projected. The experimental setup of immersion ultrasonic testing is shown in **Figure 12**. A 10 MHz
227   0.37-inch diameter - 1-inch focused transducer was used for pulse-echo measurement. A
228   pulser/receiver was connected to the transducer. Pulser/receiver simultaneously transmits and
229   receives the signal. A data acquisition system was used to collect the data. The scan area of the
230   composite plate is shown in **Figure 13**. A 2-inch by 2-inch area was scanned first for detecting the
231   manufacturing damage and flaws in the composite plates. **Figure 14** shows the C-scan image before
232   the impact event. It can be seen clearly from the figure that there are no significant manufacturing
233   defects, damage or flaws in the composite plate.   **Figure 15** shows the C-scan image after the high-
234   energy impact event. There are two high-energy impact events at location R1 and R2.   A 1-inch by
235   1-inch area was scanned first for visualizing the defect due to a high-energy impact event. **Figure 15**
236   (a) and (b) shows the evidence of impact damage at R1 and R2 location. The size of the impact damage
237   is around 2.5 mm in diameter. From **Figure 15**(a), slight delamination can also be observed around
238   the impact location.

239
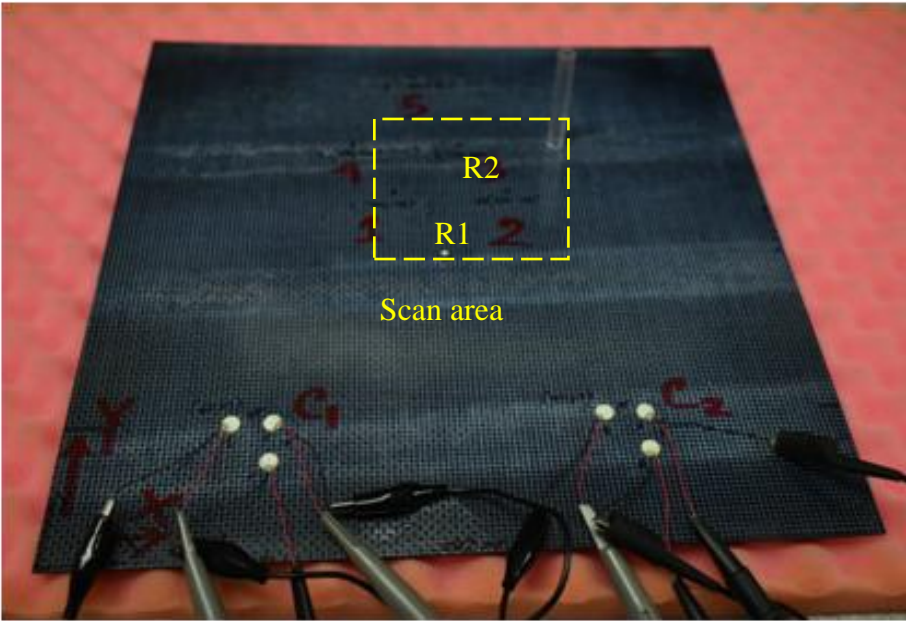
240   **Figure 13.** Scan area of the composite plate for immersion ultrasonic inspection

241
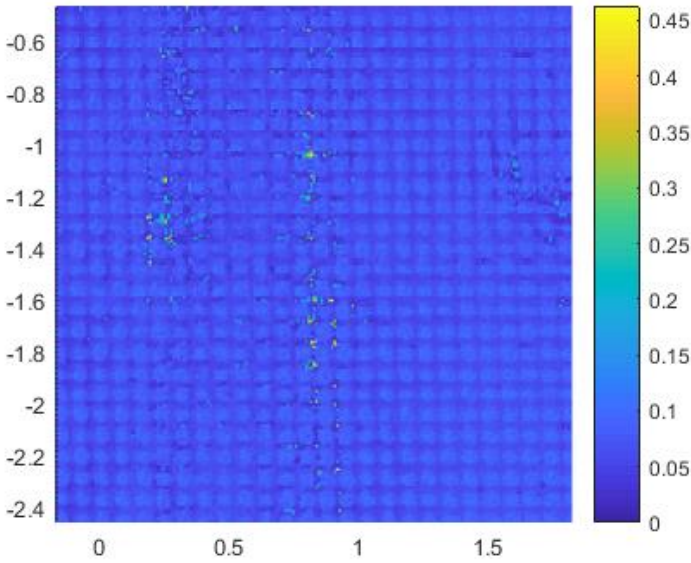
242   **Figure 14.**   C-scan image of the composite plate for manufacturing defect inspection

243

(a)   (b)
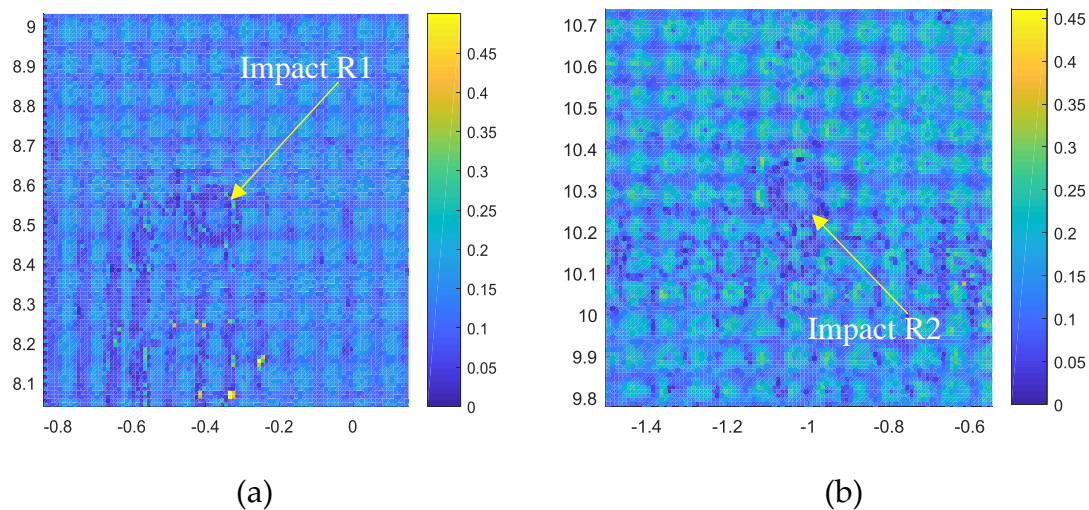
244 **Figure 15.** C-scan image of the composite plate after high-energy impact event (a) impact at R1
245 location (b) impact at R2 location

246 **5. Conclusions**

247   A compression molding process with a proper cure cycle can be used for manufacturing a
248 composite plate without any significant internal defect. We found that the manufactured plate had a
249 minimal to no defect that can affect the impact detection and localization. Piezoelectric wafer active
250 sensors can be permanently bonded to the composites to detect and localize an impact event. A
251 wavelet transform based signal processing can accurately determine the time of flight of the acoustic
252 signals. The proposed SHM technique can successfully be implemented in practice to monitor impact
253 damage. We found that the experimental measurements are in good agreement with actual impact
254 localization. An immersion ultrasonic scanning method can be used for fast inspection of internal
255 damage in a manufactured plate. There is no significant manufacturing damage was found. After the
256 high-energy impact, a clear impact damage was observed in the c-scan image.

257 **Acknowledgment**

258 Support from the National Aeronautics and Space Administration (NASA) and USC McNair center
259 are thankfully acknowledged.

260 **References**

261 1. O. Zabihi, M. Ahmadi, S. Nikafshar, K. Chandrakumar Preyeswary, M. Naebe, A technical review on
262   epoxy-clay nanocomposites: Structure, properties, and their applications in fiber reinforced composites,
263   Compos. Part B Eng. 135 (2018) 1–24. doi:https://doi.org/10.1016/j.compositesb.2017.09.066.
264 2. L. Molent, C. Forrester, The lead crack concept applied to defect growth in aircraft composite structures,
265   Compos. Struct. 166 (2017) 22–26. doi:https://doi.org/10.1016/j.compstruct.2016.12.076.
266 3. M.F. Haider, P.K. Majumdar, S. Angeloni, K.L. Reifsnider, Nonlinear anisotropic electrical response of
267   carbon fiber-reinforced polymer composites, J. Compos. Mater. (2017) 21998317719999.
268   doi:10.1177/0021998317719999.
269 4. Raihan, Rassel, Jon-Michael Adkins, Jeffrey Baker, Fazle Rabbi, and Kenneth Reifsnider. "Relationship of
270   dielectric property change to composite material state degradation." Composites Science and
271   Technology 105 (2014): 160-165.
272 5. F. Ciampa, M. Meo, A new algorithm for acoustic emission localization and flexural group velocity
273   determination in anisotropic structures, Compos. Part A Appl. Sci. Manuf. 41 (2010) 1777–1786.
274   doi:https://doi.org/10.1016/j.compositesa.2010.08.013.

275   6.   T. Kundu, Acoustic source localization, Ultrasonics. 54 (2014). doi:10.1016/j.ultras.2013.06.009.

276   7.   K.-H. Ip, Y.-W. Mai -, S.S. Kessler, S. Mark Spearing, C. Soutis, Damage detection in composite materials
277   using Lamb wave methods, 2002.

278   8.   V. Giurgiutiu, Structural Health Monitoring with Piezoelectric Wafer Active Sensors (Second Edition),
279   Academic Press, Oxford, 2014. doi:http://dx.doi.org/10.1016/B978-0-12-418691-0.00020-4.

280   9.   X.P. Qing, S.J. Beard, A. Kumar, T.K. Ooi, F.-K. Chang, Built-in Sensor Network for Structural Health
281   Monitoring of Composite Structure, J. Intell. Mater. Syst. Struct. 18 (2006) 39–49.
282   doi:10.1177/1045389X06064353.

283   10.   J.E. Michaels, T.E. Michaels, Guided wave signal processing and image fusion for in situ damage
284   localization in plates, Wave Motion. 44 (2007) 482–492. doi:10.1016/j.wavemoti.2007.02.008.

285   11.   J. Bergman, H. Chung, V. Janapati, I. Li, A. Kumar, S. Kumar-Yadav, D. Chapman, A. Nissan, R. Sarrafi-
286   Nour!, Evaluation of the Real-Time Active Pipeline Integrity Detection System for Corrosion
287   Quantification, Corros. 2016. (2016).

288   12.   A. Tobias, Acoustic-emission source location in two dimensions by an array of three sensors, Non-
289   Destructive Test. 9 (1976) 9–12. doi:https://doi.org/10.1016/0029-1021(76)90027-X.

290   13.   M.Y. Bhuiyan, V. Giurgiutiu, The signatures of acoustic emission waveforms from fatigue crack advancing
291   in thin metallic plates, Smart Mater. Struct. 27 (2017) 1–15. doi:https://doi.org/10.1088/1361-665X/aa9bc2.

292   14.   A. Ebrahimkhanlou, S. Salamone, A probabilistic framework for single-sensor acoustic emission source
293   localization in thin metallic plates, Smart Mater. Struct. 26 (2017) 95026.

294   15.   J. Frieden, J. Cugnoni, J. Botsis, T. Gmür, Low energy impact damage monitoring of composites using
295   dynamic strain signals from FBG sensors – Part I: Impact detection and localization, Compos. Struct. 94
296   (2012) 438–445. doi:10.1016/J.COMPSTRUCT.2011.08.003.

297   16.   F. Ciampa, M. Meo, Impact detection in anisotropic materials using a time reversal approach, Struct. Heal.
298   Monit. An Int. J. 11 (2012) 43–49. doi:10.1177/1475921710395815.

299   17.   S. Salamone, I. Bartoli, P. Di Leo, F.L. Di Scala, A. Ajovalasit, L. D'Acquisto, J. Rhymer, H. Kim, High-
300   velocity Impact Location on Aircraft Panels Using Macro-fiber Composite Piezoelectric Rosettes, J. Intell.
301   Mater. Syst. Struct. 21 (2010) 887–896. doi:10.1177/1045389X10368450.

302   18.   T. Kundu, S. Das, S.A. Martin, K. V Jata, Locating point of impact in anisotropic fiber reinforced composite
303   plates, Ultrasonics. 48 (2008) 193–201. doi:https://doi.org/10.1016/j.ultras.2007.12.001.

304   19.   J. Jiao, C. He, B. Wu, R. Fei, X. Wang, A new acoustic emission source location technique based on wavelet
305   transform and mode analysis, Front. Mech. Eng. China. 1 (2006) 341–345. doi:10.1007/s11465-006-0006-4.

306   20.   M. Faisal Haider, M.Y. Bhuiyan, B. Poddar, B. Lin, V. Giurgiutiu, Analytical and experimental investigation
307   of the interaction of Lamb waves in a stiffened aluminum plate with a horizontal crack at the root of the
308   stiffener, J. Sound Vib. 431 (2018) 212–225. doi:10.1016/j.jsv.2018.06.018.

309   21.   A. Baghalian, S. Tashakori, V.Y. Senyurek, D. McDaniel, H. Fekrmandi, I.N.. Tansel, Non-Contact
310   Quantification of Longitudinal and Circumferential Defects in Pipes using the Surface Response to
311   Excitation (SuRE) Method, Int. J. Progn. Heal. Manag. 8 (2017) 1–8.

312   22.   Haider, M. F., Giurgiutiu, V., Lin, B., & Yu, L. (2017). Irreversibility effects in piezoelectric wafer active
313   sensors after exposure to high temperature. *Smart Materials and Structures*, *26*(9), 095019.

314   23.   T. Kundu, A new technique for acoustic source localization in an anisotropic plate without knowing its
315   material properties, in: 6th Eur. Work. Struct. Heal. Monit., Dresden, Germany, 2012.

316   24.   A. Migot, V. Giurgiutiu, Impact Localization on a Composite Plate With Unknown Material Properties
317   Using PWAS Transducers and Wavelet Transform, in: ASME Conf. Smart Mater. Adapt. Struct. Intell. Syst.,
318   Tampa, FL, 2017: pp. 1–8.

319   25.   C.H. Wang, J.T. Rose, F.-K. Chang, A synthetic time-reversal imaging method for structural health
320   monitoring, Smart Mater. Struct. 13 (2004) 415–423. doi:10.1088/0964-1726/13/2/020.

321   26.   Vallen-System, GmbH. (2001), (n.d.). http://www.vallen.de/wavelet/index.html, Munich, Germany.

322